

Authentication by Location Tracking in Underwater Acoustic Networks

Gianmaria Ventura, *Student Member, IEEE*, Francesco Ardizzon, *Member, IEEE*,
and Stefano Tomasin, *Senior Member, IEEE*

Abstract—Physical layer message authentication in underwater acoustic networks (UWANs) leverages the characteristics of the underwater acoustic channel (UWAC) as a fingerprint of the transmitting device. However, as the device moves its UWAC changes, and the authentication mechanism must track such variations. In this paper, we propose a context-based authentication mechanism operating in two steps: first, we estimate the position of the underwater device, then we predict its future position based on the previously estimated ones. To check the authenticity of the transmission, we compare the estimated and the predicted position. The location is estimated using a convolutional neural network taking as input the sample covariance matrix of the estimated UWACs. The prediction uses either a Kalman filter or a recurrent neural network (RNN). The authentication check is performed on the squared error between the predicted and estimated positions. The solution based on the Kalman filter outperforms that built on the RNN when the device moves according to a correlated Gauss-Markov mobility model, which reproduces a typical underwater motion.

Index Terms—Location estimation, location prediction, physical layer authentication, underwater acoustic channel, physical layer security.

I. INTRODUCTION

RECENTLY, interest in underwater acoustic networks (UWANs) has grown due to their application in contexts such as natural resources extraction, ocean exploration, military operations, climate change monitoring, and marine pollution control. However, as UWAN applications become more popular, security concerns also increase.

UWAN attacks can range from simple signal jamming to impersonation attacks [1], [2]. The first solution to prevent potential attacks is to employ security protocols based on cryptography. These however have a higher communication overhead, further reducing the already low rate of data transmissions in UWAN. In this context, physical layer-based solutions that leverage the underwater acoustic channel (UWAC) characteristics provide an interesting alternative, due to their minimal overhead and utilization of UWAC features already

needed for communication purposes. The current authentication strategies for underwater acoustic communication have been surveyed in [3].

This paper focuses on authenticating messages exchanged between underwater devices with mechanisms operating at the physical layer. Physical-layer authentication techniques are trust models based on ad-hoc chosen metrics, acting as fingerprints. The underlying assumption is that the statistical distribution of the security metrics depends on transmitter and receiver positions. Thus, the source can be authenticated by verifying the match between the metrics and their expected statistic. Moreover, in this scenario, it is unrealistic to assume any knowledge of the attacker challenge distribution, as it is directly linked to the attacker’s movement, which typically remains unknown.

In [4], the authors proposed a set of metrics that are stable over time but not over space, thus a small shift in the transmitter/receiver’s position causes relevant metric variations. Next, the metrics’ distributions are estimated using a generalized Gaussian model. The model is later used to verify the channel authenticity by a generalized likelihood ratio test. Additionally, the authors propose relying on node collaboration to improve performance.

Other metrics have been proposed in [5]–[7]. In particular, the measured angle of arrival has been used in [5], the so-called time-reversal resonating strength in [6], while the maximum and the minimum correlation with of the measured channel impulse response with respect to a previously collected (positive only) dataset is studied in [7]. Concerning the method to verify the authenticity of the measurements, a common trend is to avoid the complex metrics’ distribution estimation in favor of data-driven machine learning (ML)-based checks [8]–[10]. Authentication of a moving transmitter poses further challenges, as both channel and metric distribution change over time. A typical solution is then to frame this problem as anomaly detection, where the channel is continuously monitored, and unexpected behaviors and discontinuities are associated with the start of an attack.

Along this line of research, the authors proposed in [11] a Kalman-based predictor to estimate the source position and velocity by tracking the power-weighted average of the channel taps delay, and the innovation of the Kalman filter is used to perform source authentication. The work was further extended in [12], where the Kalman filter is replaced by a recurrent neural network (RNN) to track the evolution of harder-to-estimate features. A similar approach is also proposed in [13], where the security metric is the time-of-arrival tracked by a

Manuscript received –; accepted –. Date –; date of current version –. Corresponding author: G. Ventura. This work was sponsored in part by the NATO Science for Peace and Security Programme under grant no. G5884 (SAFE-UComm). This work was also partially supported by the European Union under the Italian National Recovery and Resilience Plan (PNRR) of NextGenerationEU, partnership on “Telecommunications of the Future” (PE0000001 - program “RESTART”). The authors are with the Department of Information Engineering, Università degli Studi di Padova, Padua 35131, Italy. S. Tomasin is also with the National Inter-University Consortium for Telecommunications (CNIT), 43124 Parma, Italy. (email: gianmaria.ventura@phd.unipd.it, francesco.ardizzon@phd.unipd.it, stefano.tomasin@unipd.it).

Kalman filter.

In this paper, instead, we propose a context-based authentication mechanism. This process involves explicitly determining the source position by tracking the device’s movement and utilizing location as contextual information. Indeed, the device positions and thus its relative distance is valuable information that can also be exploited for other purposes beyond authentication, e.g., at the MAC layer for data transmission scheduling or for signal beamforming.

Thus, concerning localization in the underwater acoustic context, early works utilize the matched field processing (MFP) technique [14] to compare the measured acoustic pressure field with a local replica. This technique relies on the knowledge of the signal propagation model that, in turn, may be dependent on environmental factors and on the source position to be estimated. However, obtaining this information may be challenging in many practical scenarios.

ML models have emerged as recent solutions since source localization can be seen as a regression problem. These methods are data-driven and eliminate the need for environmental information or propagation models. The dataset can be collected from previously conducted experiments or simulators, such as Bellhop ray tracer [15]. In [16], neural network (NN), support vector machine (SVM), and random forest techniques were exploited to predict the source range by taking as input the normalized sample covariance matrix (SCM) of complex acoustic pressure in the frequency domain. Indeed, such approaches often outperform the MFP-based solution. Other localization methods are based on generalized regression neural network (GRNN) [17], convolutional neural network (CNN) [18]–[20], and RNN for both the underwater and more general communication contexts [21]–[23].

In this paper, we introduce a novel source position prediction method exploiting an array of hydrophones. Such position estimation is then exploited for authentication purposes, following a context-based authentication approach. For localization, a CNN is used to localize the source from the receivers’ measurements. The SCM is selected as input to the CNN as it compactly represents the spatial and frequency correlation between the receivers. Concerning the position tracker, two approaches have been considered, a Kalman filter and a RNN-based predictor, trained to predict the current position based on past ones. For authentication, first, we employ a predictor to estimate the current location from the past ones. Then we compute the squared error between the predicted and observed positions. The selected metric is compared to a suitably chosen threshold to check authentication.

More in detail, the paper’s main contributions are as follows.

- 1) We propose a lightweight CNN that, rather than only measuring its distance, localizes the transmitter by using the covariance matrix of the channel frequency response measured by each sensor.
- 2) We design novel predictors to track the transmitter trajectory, namely a Kalman filter-based and an RNN-based predictor. The two predictors show similar performances.
- 3) We exploit the predicted source position to distinguish between an authentic transmitter and an attacker.

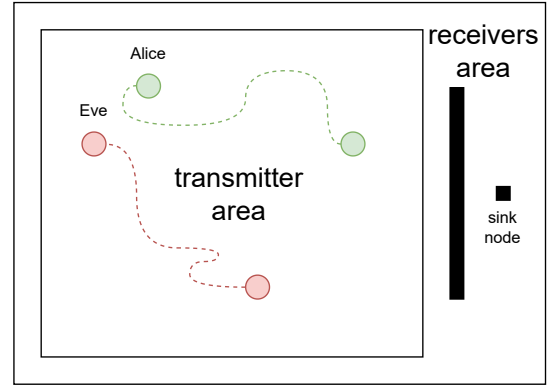


Fig. 1: Example of Alice, Bob, and Eve’s positions and movements.

- 4) We test the proposed solution using a dataset generated via Bellhop, also modeling complex environmental characteristics such as water pH and temperature.

The rest of the paper is organized as follows. Section II describes the system model. Section III presents the proposed authentication protocol. Section IV details the simulation’s setup and the localization and authentication results. Finally, Section V draws the conclusions.

II. SYSTEM MODEL

We consider an UWAN composed of one transmitter e.g., a drifter or an autonomous underwater vehicle, Alice, and a set of N_{rx} static receivers, named Bob. All receivers are synchronized and connected to a *sink node* via an error-free, authenticated, and integrity-protected channel, used only to share their observations. Next, we consider a malicious transmitter, Eve that moves in the same area.

We consider a scenario where Bob may receive messages from Alice or Eve. Eve is transmitting messages impersonating Alice, thus pretending that her messages are coming from Alice, e.g., by placing Alice’s address in her message data. Bob aims to verify if the received messages have been transmitted by Alice. To perform authentication, Bob exploits the estimate of the transmission channel over which messages are received. Such a channel depends on the position of the transmitter thus operating as its fingerprint.

For the sake of simplicity, we assume all the devices to be placed at depth d , thus a device position is uniquely identified by two Cartesian coordinates. Such a setting can be easily generalized to a three-dimensional (3D) problem, at the cost of a more involved notation. Specifically, we denote the source position, speed, and acceleration as the vectors $\mathbf{p} = (x \ y)$, $\mathbf{v} = (v_x \ v_y)$, and $\mathbf{a} = (a_x \ a_y)$, respectively. Fig. 1 shows an example of device positions and movements.

All devices communicate through a broadband UWAC with bandwidth B centered at frequency f_0 . The transmission band is split into K sub-bands and the channel is assumed to be narrowband within each sub-band. We denote with $H_{r,k}$ ($G_{r,k}$) the complex baseband equivalent narrowband channel between Alice (Eve) and receiver $r \in [1, N_{rx}]$, for sub-band k centered

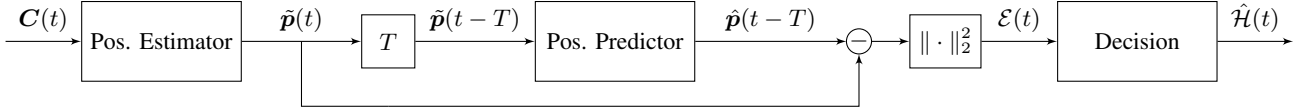


Fig. 2: Workflow of the proposed source localization and authentication protocol.

at frequency f_k . The noisy channel for receiver r at sub-band k is modeled as

$$Q_{r,k} = w_{r,k} + \begin{cases} H_{r,k}, & \text{if Alice is transmitting,} \\ G_{r,k}, & \text{if Eve is transmitting,} \end{cases} \quad (1)$$

We collect the noisy channel gains of sub-band k for every receiver into the column vector

$$\mathbf{Q}_k = (Q_{1,k}, \dots, Q_{r,k}, \dots, Q_{N_{rx},k})^T, \quad (2)$$

and define its normalized counterpart as

$$\tilde{\mathbf{Q}}_k = \frac{\mathbf{Q}_k}{\|\mathbf{Q}_k\|_2}, \quad (3)$$

where $\|\mathbf{Q}_k\|_2$ is the norm-2 of the vector.

The sink node computes the SCM at frequency f_k as

$$\mathbf{C}_k = \tilde{\mathbf{Q}}_k \tilde{\mathbf{Q}}_k^\dagger, \quad (4)$$

where \dagger is the Hermitian conjugate operator. Finally, it arranges the SCMs in the 3D matrix

$$\mathbf{C} = (\mathbf{C}_1; \dots; \mathbf{C}_K), \quad (5)$$

where semicolons separate the matrices in the third dimension. We then build a dataset of M consecutively sampled \mathbf{C} when the source is moving. Such a dataset will be later used to train the NNs.

A. Security Model

Here, we detail the considered security model, which also includes the assumptions made on attacker Eve. We consider the worst-case scenario where, when Eve transmits, Bob receives messages only from her. For instance, such a condition can be obtained when Eve transmits at a higher power than Alice, or Eve waits for time slots when Alice is not transmitting.

We assume Eve to know both Alice's and Bob's positions. On the other hand, Eve must be far at least D from Alice to not be detected by Alice, modeling for example the use of sonar by Alice. Still, Eve is capable of tracking and estimating Alice's movement. Thus, we will consider attacks where Eve tries to impersonate Alice by transmitting to Bob while mimicking Alice's motion pattern.

At an initial stage, Alice can transmit N_a pilot signals that are authenticated by higher-layer mechanisms and are thus unpredictable. Such initial secure transmission is used to obtain the first set of authenticated features and then exploited to authenticate forthcoming transmission using only physical-layer features. Indeed, using a cryptographic authentication protocol adds communication overhead and computational complexity.

During training, we assume that signals are protected by a higher-layer authentication mechanism, thus preventing adversarial (pollution) attacks. Moreover, we remark that such

an attack would require the pre-compensation of all the N_{rx} channels from Eve to each receiver at the same time, which may be unfeasible in practice. On the other hand, even if Eve could imitate all the channels, the proposed mechanism would still be secure, since, for an effective attack, Eve should still perfectly predict and replicate Alice's movements.

Finally, since the communication between each receiver is authenticated, Eve can interfere only before the receivers' front end.

III. PROPOSED AUTHENTICATION PROTOCOL

The proposed authentication protocol relies on the samples' temporal correlation. To authenticate a transmission, Bob performs M estimates of the UWAC. While, for the sake of simplicity, we assume that Bob performs its UWAC estimates at regular time intervals spaced by T , the proposed models could be modified to work with irregular time series. Thus, at each instant $t = \ell T$, $\ell = 1, \dots, M$, a new packet is transmitted (by either Alice or Eve) and received by the set of hydrophones Bob.

At an initial stage, Alice is transmitting N_a packets to be used to obtain the first set of authenticated features and then exploited by the proposed authentication protocol.

In particular, when receiving a new message at time $t > N_a T$, Bob

- 1) predicts the position $\hat{\mathbf{p}}(t) = (\hat{x}(t) \hat{y}(t))$ from $\tilde{\mathbf{p}}(t - T)$, using the solutions described in Sections III.B and III.C;
- 2) estimates $\mathbf{C}(t)$ from the UWAC, as detailed in Section II and feeds it as input to the position estimator (described in Section III.A), which in turn outputs $\tilde{\mathbf{p}}(t) = (\tilde{x}(t) \tilde{y}(t))$;
- 3) computes the squared error between the predicted and estimated positions as

$$\mathcal{E}(t) = \|\hat{\mathbf{p}}(t) - \tilde{\mathbf{p}}(t)\|_2^2; \quad (6)$$

- 4) decides about the authenticity of the received message according to the following test

$$\hat{\mathcal{H}}(t) = \begin{cases} 0, & \text{if } \mathcal{E}(t) < \lambda, \\ 1, & \text{if } \mathcal{E}(t) \geq \lambda, \end{cases} \quad (7)$$

where $\hat{\mathcal{H}}(t) = 0$ means that the received message has been recognized as authentic (coming from Alice) and $\hat{\mathcal{H}}(t) = 1$ means that the received message has been recognized as fake (coming from Eve).

Fig. 2 shows a block scheme of the proposed authentication protocol.

Called $\mathcal{H}(t) = 0$ the legitimate case and $\mathcal{H}(t) = 1$ the under-attack case, i.e., when Eve is transmitting, the overall aim of our authentication technique is to minimize the missed detection (MD) probability

$$p_{MD}(t) = P(\hat{\mathcal{H}}(t) = 0 | \mathcal{H}(t) = 1), \quad (8)$$

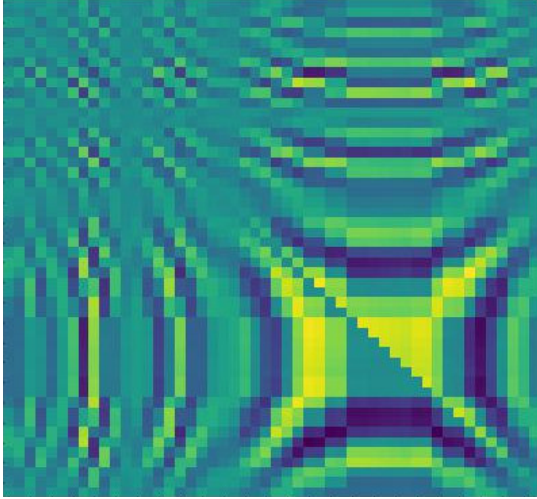


Fig. 3: Example of processed SCM heatmap \hat{C}_k .

for a fixed false alarm (FA) probability

$$p_{\text{FA}}(t) = P\left(\hat{H}(t) = 1 | H(t) = 1\right). \quad (9)$$

We remark that the computational cost of this solution is due to both training and inference. Only the former requires multiple function evaluations; however, it is performed once and may be run on a dedicated device, e.g., designed only for this task. The cost of each single evaluation is due only to the number of parameters of the NN. Thus, to limit the impact of the proposed authentication mechanism computational cost, we will look at solutions with a limited number of parameters.

In the remaining part of this Section, we will detail the designed position estimator and the position predictor blocks.

A. Position Estimation

The task of the position estimator is to match the SCMs C to the source position. This can be modeled as a regression problem that we tackle with a CNN.

Before feeding the data to the CNN we perform the following processing. First, we extract the upper triangular part of each matrix $C_k(t)$ as $U_k(t)$. Then, we build the full real-value matrix

$$\hat{C}_k(t) = \Re(U_k(t)) + \Im(U_k(t))^T, \quad (10)$$

where $\Re(\cdot)$ and $\Im(\cdot)$ extract the real and imaginary parts of their argument, respectively. Next, we normalize the obtained matrix to have zero mean and unitary variance. An example of such a matrix is shown in Fig. 3.

The processed 3D matrix

$$\hat{C}(t) = \left(\hat{C}_1(t); \dots; \hat{C}_K(t)\right) \quad (11)$$

is then used as input for the developed CNN.

To solve the regression problem a CNN called localization network (LOC-NET) is now introduced. The driving idea is that K covariance matrices can be treated as an image having K channels, instead of the 3 in RGB images. Indeed, a CNN can exploit the spatial and channel (i.e., the frequency) correlation in image-like input data. Inspired by the CNN developed in [20], which is based on the Xception [24] network for image

classification, we introduce the LOC-NET architecture. We remark that LOC-NET is a novel architecture, as it inherits only the convolutional block structure from the other CNN. Additionally, we do not use residual connections since LOC-NET is much smaller than the CNN of [20]. Furthermore, the smaller NN yields faster and easier training and makes it suitable for UWANs.

LOC-NET Architecture: In the CNN LOC-NET, each convolutional block is composed of:

- a 2D convolutional layer,
- a batch normalization layer,
- a ReLu activation function,
- a dropout layer.

Using convolutional layers instead of dense layers reduces the number of learnable parameters while the batch normalization layer avoids the internal covariate shift and makes the training faster and more stable [25]. ReLu's are selected as the standard activation functions in CNN [26] while the dropout layer prevents overfitting during the training procedure [27] and improves the network generalization abilities. The output of the CNN $\tilde{p}(t)$ is an estimate of the transmitter position at time t , $p(t)$.

LOC-NET Training: During the training, the CNN is expected to learn the map between each source position and SCMs. To this end, we assume to have a database containing both $C(t)$ and the corresponding true position $p(t)$. For this regression problem, we consider as loss function the mean squared error (MSE)

$$l = \frac{1}{b} \sum_{i=1}^b (x_i - \tilde{x}_i)^2 + \frac{1}{b} \sum_{i=1}^b (y_i - \tilde{y}_i)^2, \quad (12)$$

where b is the batch size and the index i represents the i -th sample of the selected batch.

In the following, we detail two alternative architectures for position prediction, one based on a Kalman filter and the other on a RNN. They both aim at predicting the location $\hat{p}(t)$ from the output of the LOC-NET $\tilde{p}(t - T)$.

B. Position Prediction by Kalman Filter

The Kalman filter provides a computational-efficient (recursive) solution based on the least-squares method [28]. The Kalman filter is unsupervised, and, differently from typical ML-based solutions, it does not need extensive training procedures. However, in general, it requires prior knowledge about the source motion and the observation model.

As described in Section II, we assume that Alice is moving on a horizontal plane at depth d . Thus, the Kalman filter tracks a transmitter moving on a 2D plane at a constant speed.

The vector of position measurements $\tilde{p}(t)^T$ collects the noisy estimates of coordinates provided by the LOC-NET. We define the hidden state vector collecting the position and speed components estimated by the Kalman filter as

$$\mathbf{h}(t) = (\hat{x}(t) \ \hat{v}_x(t) \ \hat{y}(t) \ \hat{v}_y(t))^T. \quad (13)$$

The state transition matrix F and the observation matrix O are

$$F = \begin{pmatrix} X & 0 \\ 0 & Y \end{pmatrix}, \text{ with } X = Y = \begin{pmatrix} 1 & T \\ 0 & 1 \end{pmatrix} \quad (14)$$

and

$$\mathbf{O} = \begin{pmatrix} 1 & 0 & 0 & 0 \\ 0 & 0 & 1 & 0 \end{pmatrix}. \quad (15)$$

We call the (set a priori) noise covariance matrices of process and measurement \mathbf{Q} and \mathbf{R} , respectively.

Both $\mathbf{h}(t)$ and $\mathbf{P}(t)$ have to be initialized, we set $\mathbf{h}(0) = (\tilde{x}(0) \ 1 \ \tilde{y}(0) \ 1)$ and its covariance $\mathbf{P}(0) = 10^3 \cdot \mathbb{1}_4$. At each considered time step $t = \ell T$ the following operations are performed. First, during the *time update*, the current state vector and the covariance matrix are predicted from the previous ones, as

$$\mathbf{h}(t) = \mathbf{F}\mathbf{h}(t-T), \quad (16)$$

$$\mathbf{P}(t) = \mathbf{F}\mathbf{P}(t-T)\mathbf{F}^T + \mathbf{Q}. \quad (17)$$

When a new measurement is available, during the *measurement update* step we correct the predicted state vector and the covariance matrix by using the new measurement $\tilde{\mathbf{p}}(t)^T$, as

$$\mathbf{K} = \mathbf{P}(t)\mathbf{O}^T (\mathbf{O}\mathbf{P}(t)\mathbf{O}^T + \mathbf{R})^{-1}, \quad (18)$$

$$\mathbf{h}(t) = \mathbf{h}(t) + \mathbf{K} (\tilde{\mathbf{p}}(t)^T - \mathbf{O}\mathbf{h}(t)), \quad (19)$$

$$\mathbf{P}(t) = (\mathbb{1}_4 - \mathbf{K}\mathbf{O})\mathbf{P}(t) (\mathbb{1}_4 - \mathbf{K}\mathbf{O})^T + \mathbf{K}\mathbf{R}\mathbf{K}^T, \quad (20)$$

where \mathbf{K} is called Kalman gain, which determines the amount of correction to be applied to the prediction.

Therefore, $\forall t > 0$ the predicted position can be extracted from (16) and (19) as

$$\hat{\mathbf{p}}(t) = \mathbf{O}\mathbf{F} [\mathbf{h}(t-T) + \mathbf{K} (\tilde{\mathbf{p}}(t-T)^T - \mathbf{O}\mathbf{h}(t-T))], \quad (21)$$

where $\tilde{\mathbf{p}}(t-T)^T$ is the source position estimate performed by the LOC-NET at time $t-T$.

The described Kalman filter works with regular time series of data, sampled with period T ; however, it could be adapted to work also with irregular time series of data assuming that the time intervals between one sample and the next one are known. More details concerning the Kalman filter and its statistical properties can be found in [29, Ch. 13].

C. Position Prediction by Recurrent Neural Network

To circumvent the need for the a priori knowledge of the transmitter movement's model, we consider a data-driven model based on a RNN, trained to predict the next source position $\hat{\mathbf{p}}(t)$ from the previous ones $\tilde{\mathbf{p}}(t-T)$. In this way, the model is comparable with the Kalman and improves its performance by exploiting its inner memory.

In particular, we consider a RNN comprising N_ℓ long short term memory (LSTM) layers that, with their internal memory, extract the sequences' temporal correlation, a dropout layer to avoid overfitting, and N_d dense layers.

Each LSTM layer [30] is characterized by a *state* which is updated at each new input, with period T . In particular, input sample $\tilde{\mathbf{p}}(t-T)$ is processed using state at time $t-T$, which include a *cell state* \mathbf{c}_{t-T} and a *hidden state* \mathbf{h}_{t-T} . The corresponding output of the layer is $\hat{\mathbf{p}}(t)$. Internally, first, the *input gate* \mathbf{i}_t , the *forget gate* \mathbf{f}_t , and the *cell gate* \mathbf{g}_t vectors are computed as follows. Denoting the sigmoid

and hyperbolic activation functions as σ_{act} and \tanh and the Hadamard product operator as \odot , we have

$$\mathbf{i}_t = \sigma_{\text{act}}(\mathbf{W}_{ii}\tilde{\mathbf{p}}(t-T) + \mathbf{b}_{ii} + \mathbf{W}_{hi}\mathbf{h}_{t-T} + \mathbf{b}_{hi}), \quad (22)$$

$$\mathbf{f}_t = \sigma_{\text{act}}(\mathbf{W}_{if}\tilde{\mathbf{p}}(t-T) + \mathbf{b}_{if} + \mathbf{W}_{hf}\mathbf{h}_{t-T} + \mathbf{b}_{hf}), \quad (23)$$

$$\mathbf{g}_t = \tanh(\mathbf{W}_{ig}\tilde{\mathbf{p}}(t-T) + \mathbf{b}_{ig} + \mathbf{W}_{hg}\mathbf{h}_{t-T} + \mathbf{b}_{hg}), \quad (24)$$

where \mathbf{W}_{ii} , \mathbf{W}_{if} , \mathbf{W}_{ig} , \mathbf{W}_{hi} , \mathbf{W}_{hf} , and \mathbf{W}_{hg} are weight matrices, while \mathbf{b}_{ii} , \mathbf{b}_{if} , \mathbf{b}_{ig} , \mathbf{b}_{hi} , \mathbf{b}_{hf} , and \mathbf{b}_{hg} are bias vectors. Then, the output of the layer is computed as follows

$$\hat{\mathbf{p}}(t) = \sigma_{\text{act}}(\mathbf{W}_{io}\tilde{\mathbf{p}}(t-T) + \mathbf{b}_{io} + \mathbf{W}_{ho}\mathbf{h}_{t-T} + \mathbf{b}_{ho}), \quad (25)$$

where \mathbf{W}_{io} and \mathbf{W}_{ho} are weight matrices, while \mathbf{b}_{io} and \mathbf{b}_{ho} are bias vectors.

Moreover, the cell and hidden states are updated for each input. In particular, the cell state is computed from the forget gate, which establishes how much information has to be kept from the previous cell state, the input, and the cell gate, as

$$\mathbf{c}_t = \mathbf{f}_t \odot \mathbf{c}_{t-T} + \mathbf{i}_t \odot \mathbf{g}_t. \quad (26)$$

Finally, the hidden state represents the output of the cell and is computed from both the cell state and the output gate to get direct information about the previous inputs, as

$$\mathbf{h}_t = \hat{\mathbf{p}}(t) \odot \tanh(\mathbf{c}_t). \quad (27)$$

After proper training and $\forall t > 0$, the proposed RNN takes as input the source position estimated by the LOC-NET $\tilde{\mathbf{p}}(t-T)$, and it predicts the transmitter position $\hat{\mathbf{p}}(t)$ acting in the same way as the Kalman filter.

We remark that, even if we focus on the case where the data is sampled with a constant rate, RNNs can be adapted to irregular time series, as shown in [31].

IV. NUMERICAL RESULTS

In this Section, we present the performance of the proposed solution. First, we describe the dataset generation. Then, we detail the parameter design of the employed solution. Lastly, we evaluate the localization and authentication accuracy. Note that since all existing literature has only considered the authentication in a static scenario, we do compare our solution with existing approaches, which would perform very poorly when the source is moving.

A. Dataset Generation: Bellhop Simulation

The 3D underwater acoustic simulator Bellhop [15], a beam-tracing model for simulating acoustic pressure field propagation in ocean environments, was used to generate the datasets.

Two areas of the San Diego Bay have been selected for the simulation. To confine the transmitter movement, we selected an inner area where the transmitter was allowed to move. The receivers have been located just outside of the transmitter area (see Fig. 1).

During a simulation, the source travels inside the transmitter area at depth $d = 50$ m according to a correlated Gauss-Markov mobility model. Specifically, it starts moving from a position selected uniformly at random in the area, with initial speed direction drawn uniformly random in $[0, 2\pi)$, and

modulus $v(0) = 2$ m/s. The source speed and position are then periodically updated with period $T = 10$ s as follows

$$v(t+T) = \alpha v(t) + \boldsymbol{\eta}(t)\sqrt{1-\alpha^2}, \quad (28)$$

$$\mathbf{p}(t+T) = \mathbf{p}(t) + \mathbf{v}(t)T, \quad (29)$$

where $\alpha = 1 - 2 \cdot 10^{-3}$ is the trajectory correlation factor, and $\boldsymbol{\eta}(t)$ is a 2D vector with zero-mean independent Gaussian entries and standard deviations (STDs), respectively, $\sigma_x = \sigma_y = 2$ m/s.

For each path, an acoustic signal with carrier frequency f_0 is transmitted from the source. The signal propagation is simulated through the 3D geometric beams approximation [32], which transmits beams for every couple of the selected elevation and bearing angles. Since the metrics of interest are the complex amplitudes and the delays of the channel impulse response, Bellhop is run in the so-called *arrivals mode*.

Fig. 4 shows the bathymetry used to produce the simulated dataset, where the corner with Cartesian coordinates $(0, 0)$ has coordinates $(32^\circ 52' 30'' \text{ N}, 117^\circ 19' 25'' \text{ W})$ with the x and y axis pointing respectively to the North and West. The size of the selected area is $2125 \text{ m} \times 2550 \text{ m}$, with the transmitter placed in an inner area of dimensions $1500 \text{ m} \times 2000 \text{ m}$ with corners' coordinates $(313 \text{ m}, 275 \text{ m}) - (313 \text{ m}, 2275 \text{ m}) - (1813 \text{ m}, 2275 \text{ m}) - (1813 \text{ m}, 275 \text{ m})$. Furthermore, another area of the same size, called bathymetry 2, was selected 500 m North of the previous one to validate the proposed authentication model in a different geological setting. In this setup, three different receivers' dispositions were tested:

Disp. 1 $N_{\text{rx}} = 50$ receivers are uniformly placed along the line $(1970 \text{ m}, 875 \text{ m} - 1375 \text{ m})$;

Disp. 2 $N_{\text{rx}} = 50$ receivers are uniformly placed in a u-like shape. Ten of them are at coordinates $(1970 \text{ m}, 1260 \text{ m} - 1320 \text{ m})$, twenty at $(970 \text{ m} - 1160 \text{ m}, 2410 \text{ m})$ and the remaining at $(970 \text{ m} - 1160 \text{ m}, 140 \text{ m})$;

Disp. 3 $N_{\text{rx}} = 10$ receivers are uniformly placed along the line $(1970 \text{ m}, 1230 \text{ m} - 1320 \text{ m})$.

In all dispositions, the receivers are placed at depth $d = 50$ m. The dispositions have been sketched in Fig. 4. In addition, to evaluate the proposed model's robustness to the number of available receivers disposition 1 has been modified with $N_{\text{rx}} = 20, 30, \text{ and } 40$.

Table I summarizes the parameters to be set for the Bellhop simulator. More in detail,

- the central frequency is $f_0 = 11.5$ kHz with bandwidth $B = 5$ kHz, thus accommodating the $[9, 14]$ kHz band typically employed in underwater acoustic (UWA) communications;
- the noise variance for each receiver at the desired signal to noise ratio (SNR) is computed as $\sigma_r^2 = P_r / 10^{\frac{\text{SNR}}{10}}$, where P_r is the average received power for receiver r at a distance between 200 m and 300 m from the transmitter;
- to achieve a trade-off between frequency accuracy and input data size we considered $K = 48$ frequencies;
- to ensure that the source beams reach the receivers from every position in the transmitter area we selected as

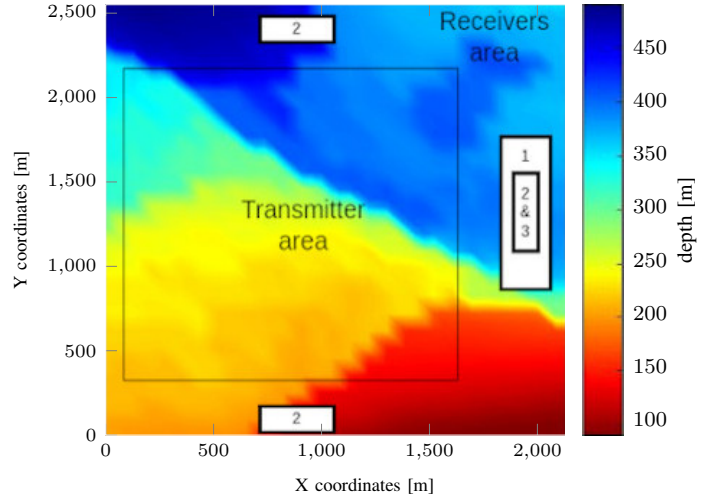


Fig. 4: Receivers' dispositions 1, 2, and 3 for Bathymetry 1.

TABLE I: Parameters for the Bellhop simulator.

Bellhop parameters	
carrier frequency	f_0
sound speed profile	Munk profile
bottom boundary	acoustic-elastic half-space
source coordinates	$\mathbf{p}(t)$
source/receiver depth	d
receivers ranges	N_{rx} distances from source
receivers bearings	N_{rx} bearing angles
run type	arrivals, 3D, geometric beams
elevation angles	25 angles, from α_1 to α_2
bearing angles	4 angles, from β_1 to β_2
bathymetry	San Diego Bay bathymetry (1 or 2)

elevation angles $\alpha_1 = -10^\circ$ and $\alpha_2 = 20^\circ$ and as bearing angles $\beta_1 = -90^\circ$ and $\beta_2 = 90^\circ$.

Each simulation is iterated for $M = 50$, hence the output of each simulation is a 50 element cell composed by $N_{\text{rx}} \times N_{\text{rx}} \times K$ complex-valued matrices.

B. Model Architectures and Training Parameters

In this Section, we detail the design parameter of the LOC-NET, i.e., the position estimator, and both Kalman filter and RNN which implement, in turn, the position predictor.

LOC-NET: After the preprocessing (see Section III), the input fed into the CNN is a tensor of size $(b, N_{\text{rx}}, N_{\text{rx}}, K)$ where $K = 48$, $b = 40$ is the selected batch size¹, and $N_{\text{rx}} = 10$ or 50 is the number of receivers. It is worth noticing that two different LOC-NET architectures are proposed for $N_{\text{rx}} = 50$ and $N_{\text{rx}} = 10$. While for $N_{\text{rx}} = 20, 30, \text{ and } 40$, the input tensor is zero-padded to keep the same CNN architecture as in the case with $N_{\text{rx}} = 50$. Moreover, since the LOC-NET learns how the transmitted signal propagates given an environment and a receiver's disposition, when the bathymetry or the receivers' disposition changes a new model has to be trained. Then the input goes through six convolutional blocks composed of different layers, as described in Section III-A. After the convolutional blocks, two dense layers provide as

¹The hyperparameter $b = 40$ was chosen via manual tuning.

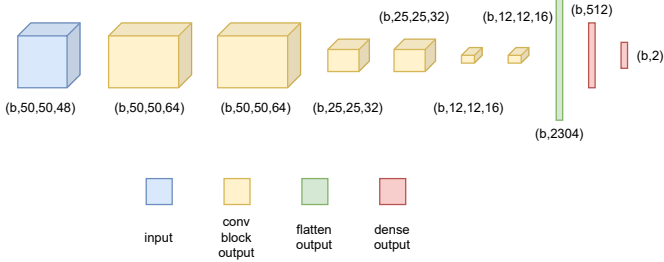


Fig. 5: LOC-NET graphical representation.

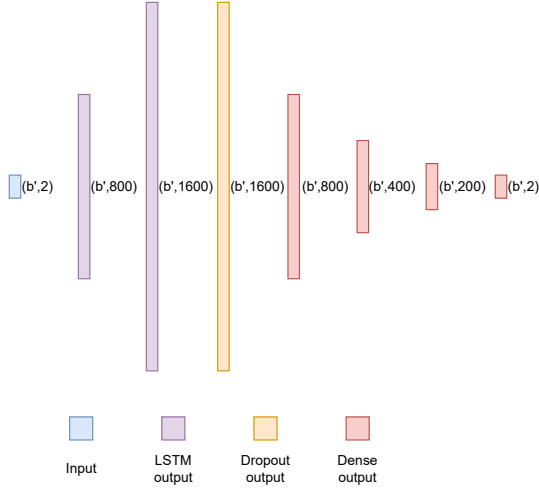


Fig. 6: RNN graphical representation.

final output a $b \times 2$ matrix, collecting the predicted source position $\hat{\mathbf{p}}$ for every sample in the considered batch. Indeed, the x and y coordinates are sufficient to identify the transmitter position as we assumed Alice can only move in the horizontal plane at depth $d = 50$ m. The architecture is sketched in Fig. 5. We remark that the proposed CNN has approximately 1.2×10^6 parameters while other CNNs performing source localization in simpler scenarios are much more complex. For example, different NN models are proposed in [17], with a number of parameters between 1.2×10^6 and 6.2×10^6 ; the NN developed in [18] has approximately 16×10^6 parameters, and the NN in [20] has even 5×10^9 parameters. Concerning the training, we used the MSE loss function (12) and the adaptive moment estimation (ADAM) optimizer with weight decay parameter 10^{-5} . The learning rate was initially set to 10^{-3} and then gradually decreased to 10^{-4} during the 300 training epochs. The best model was selected using a validation set, in this way, the generalization abilities of the model are preserved. The training and validation datasets for the LOC-NET are respectively composed of 4000 and 1000 samples.

RNN: The input of the RNN is a tensor having shape $(b', 2)$ with $b' = 8$ being the RNN's batch size optimum value. The core features of the RNN are two LSTM layers. The first has input size 2 and hidden size 800, while the second one has input size 800 and hidden size 1600. After the LSTM layer, we include a dropout layer. Then, after that, four dense layers gradually reduce the tensor shape to get an output of size $(b', 2)$. This represents the source position at the next time

TABLE II: Loc-net transmitter position error in different dispositions.

Disposition N.	1	2	3
Avg. Localization error	74 m	72 m	117 m
STD Localization error	58 m	50 m	114 m

step, for every sample in the considered batch. Again, the MSE was selected as the loss function, ADAM as optimizer with a weight decay parameter² of 10^{-3} . The learning rate of the optimizer starts again from 10^{-3} but decreases to 10^{-5} along the 300 training epochs. Finally, a validation set was included to select the best model. The training and validation datasets for the RNN, instead, are respectively composed of the LOC-NET training and validation outputs.

C. Localization Performance

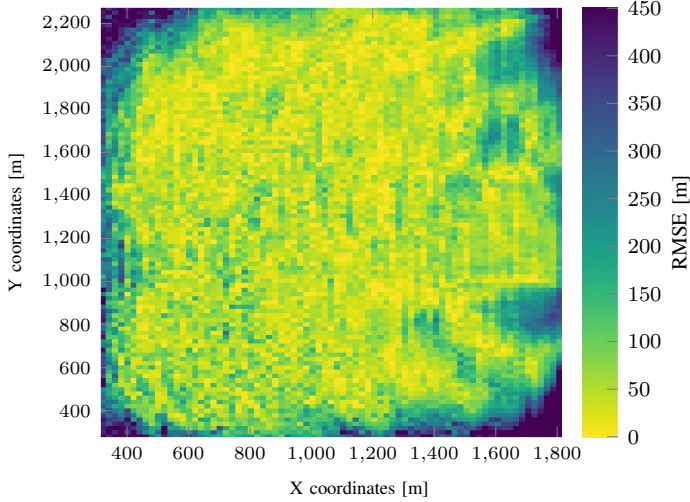
In this Section, we present the localization performance achieved by the different models described in Section III.

First, we investigate the localization performance of the LOC-NET, starting from the impact of the receivers' spatial distribution on localization. In particular, we consider the three dispositions of Section IV-A with $\text{SNR} = 20$ dB. Results are collected in Table II. As expected, dispositions 1 and 2 reach a higher accuracy than disposition 3, due to the higher number of receivers, i.e., $N_{\text{rx}} = 50$ vs. $N_{\text{rx}} = 10$. Still, when looking at applications with stricter constraints on N_{rx} , it may be possible to seek an optimal tradeoff between the number of used receivers and the localization error. On the other hand, the similar average position errors achieved for dispositions 1 and 2 suggest that the geometric disposition of the receivers has a limited impact on the performance of the proposed estimator.

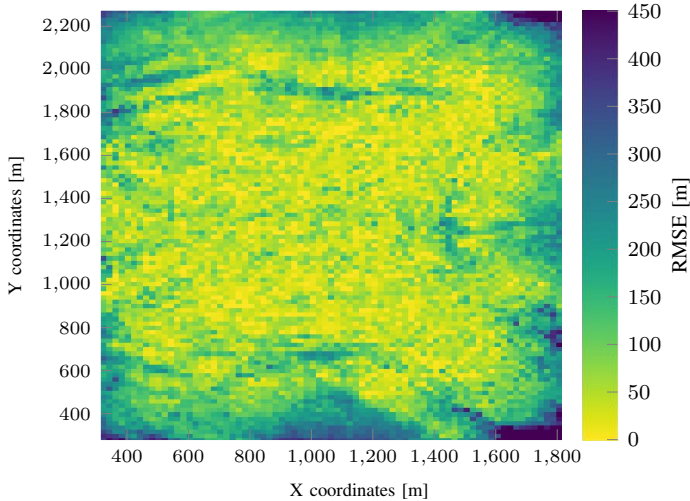
To further investigate the spatial distribution of errors, Fig. 7 shows the localization errors of the LOC-NET, as a function of the transmitter position. In particular, the color of each point represents the magnitude of the LOC-NET localization error achieved when the source transmits from that point. From Fig. 7a we observe that the transmitter positions leading to the larger errors are around the four corners, i.e., either locations almost aligned with the receiver line (right corners) or too far away from the receivers (left corners). Additionally, a wave-like behavior in the error is observed, parallel to the receivers' position. This confirms the idea that sources placed close along the y -axis will be hardly distinguished, due to the particular receiver placement. Concerning disposition 2, reported in Fig. 7b, where the receivers are arranged in a u-shape around the transmitter area, while the highest errors are placed again at the corners, the error appears to be slightly more uniformly distributed. Still, in conclusion, we can state that higher errors occur when the transmitter is too far or too aligned with the receiver line.

Fig. 8 shows (in box plots) the error distributions for the localization task as a function of the SNR, for $\text{SNR} = 0, 10,$ and 20 dB. As expected, the average accuracy improves with

²Lower values led to model overfitting.



(a) Disposition 1



(b) Disposition 2

Fig. 7: LOC-NET error heatmaps for disposition 1 and 2, for all the possible source positions.

increasing SNR furthermore, this leads to a decrease in the error confidence interval.

To assess the localization accuracy of the standalone predictor block, we generated a trajectories dataset of source positions following the mobility model described in Section IV-A. In detail, we considered

$$\mathbf{p}^*(t) = \mathbf{p}(t) + \mathbf{w}_{\text{pos}}, \quad (30)$$

where $\mathbf{p}(t)$ is the true trajectory, simulated as in (29), and \mathbf{w}_{pos} is a Gaussian stationary noise with zero mean and STD values equal on each component σ_{pos} , modeling the uncertainty introduced by the position estimator. In particular, we considered as possible STDs $\sigma_{\text{pos}} = 25, 50, \text{ and } 100$ m. Then both the RNN and the Kalman filter were tested receiving as input trajectories $\mathbf{p}^*(t)$.

As shown in Fig. 9, the proposed predictors achieve similar performance in mean at a high STD σ_{pos} .

We now consider the localization performance at the output of the position predictor block obtained using the LOC-NET

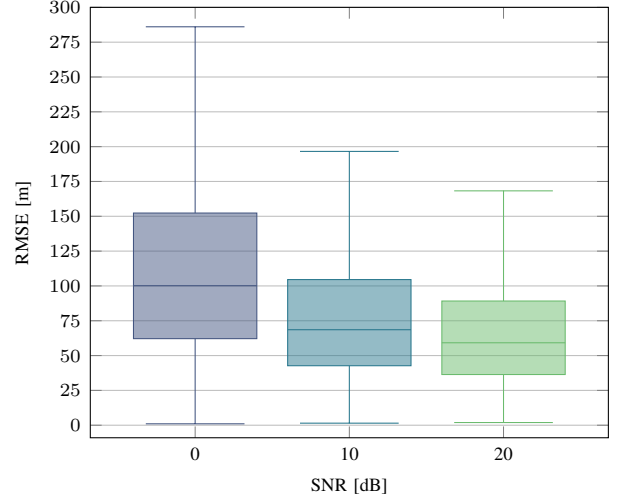


Fig. 8: Transmitter position errors distribution achieved by the LOC-NET, for different values of SNR.

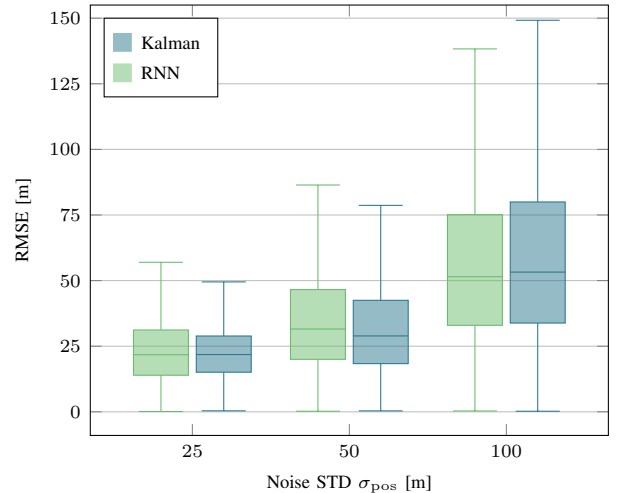


Fig. 9: Transmitter position errors of Kalman and RNN, receiving as input noisy source trajectories, with position estimation noise σ_{pos} .

as the position estimator. Fig. 10 collects the results for $\text{SNR} = 20$ dB. Both the Kalman filter and the RNN improve the performance of the LOC-NET since they rely on the time sequence correlation to correct and smooth the localization errors induced by the LOC-NET. In addition, it can be noticed that the RNN achieves a slightly lower prediction error.

The numerical metrics reported in Table III, besides highlighting the great average results of the proposed estimator and predictors, confirm the fact that both RNN and Kalman filter improve the LOC-NET estimates, achieving almost the same

TABLE III: Estimated localization errors with $\text{SNR} = 20$ dB.

Loc. Model	x RMSE	y RMSE	x MAPE	y MAPE
LOC-NET only	72.7 m	63.1 m	5.8%	4.9%
LOC-NET + Kalman	63.4 m	54.7 m	4.9%	4.1%
LOC-NET + RNN	60.8 m	55.5 m	4.6%	4.1%

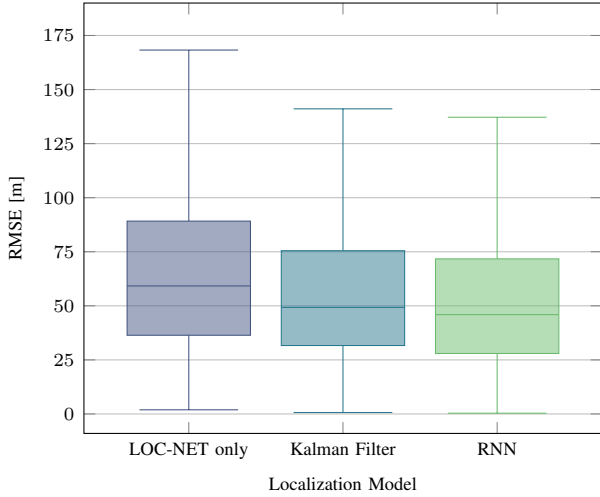


Fig. 10: Transmitter position errors of LOC-NET, Kalman, and RNN with SNR = 20 dB.

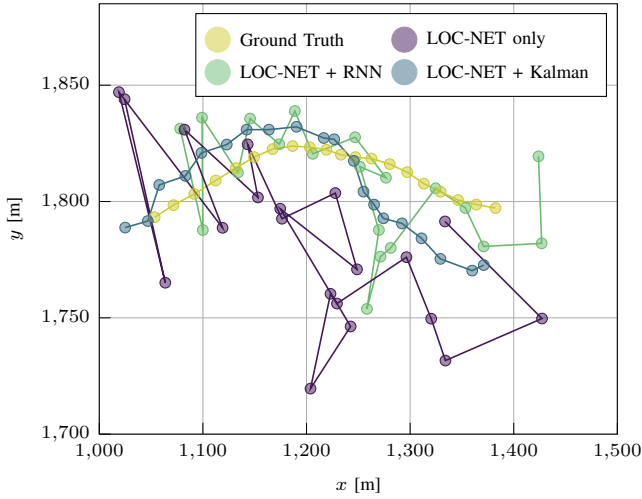


Fig. 11: Example of localized transmitter position using LOC-NET only, LOC-NET + Kalman, and LOC-NET + RNN, with SNR = 20 dB.

root mean square error (RMSE) and mean absolute percentage error (MAPE) in estimating the source coordinates. Still, we remark that the Kalman filter is less general than the RNN since it requires an a priori knowledge about the nature of the source motion. In this sense, it has an inherent advantage over the RNN, which has instead no a priori knowledge about the source motion model plugged in.

The effect of such knowledge is shown in Fig. 11, where the Kalman filter predictions are equally spaced and resemble the trajectory of the real source motion. This is because the Kalman filter forces the source motion model on the output, thus outputting a trajectory that is close to the ground truth since the real transmitter motion can be well approximated by a constant speed motion model. On the other hand, the source positions predicted by the RNN do not have the same shape, as the RNN only works using the LOC-NET (noisy) output. Still, this highlighted the effectiveness of the proposed approach that, even with an inherent disadvantage, it can achieve a slightly more accurate localization.

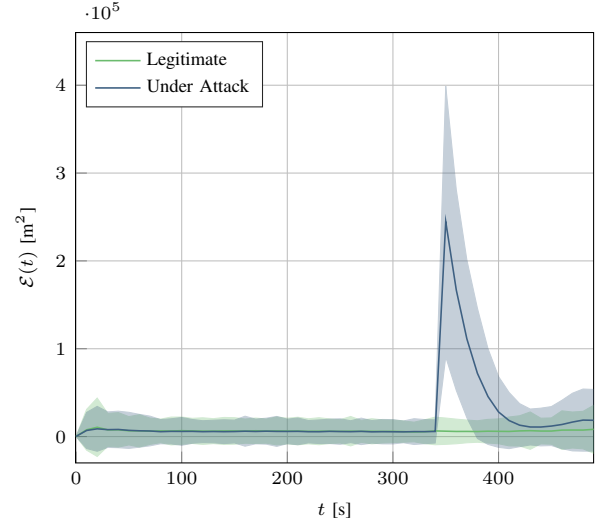


Fig. 12: Mean and 2σ confidence intervals of $\mathcal{E}(t)$, for the Kalman filter in the legitimate and under-attack (starting from $t = 350$ s) scenarios, for SNR = 20 dB.

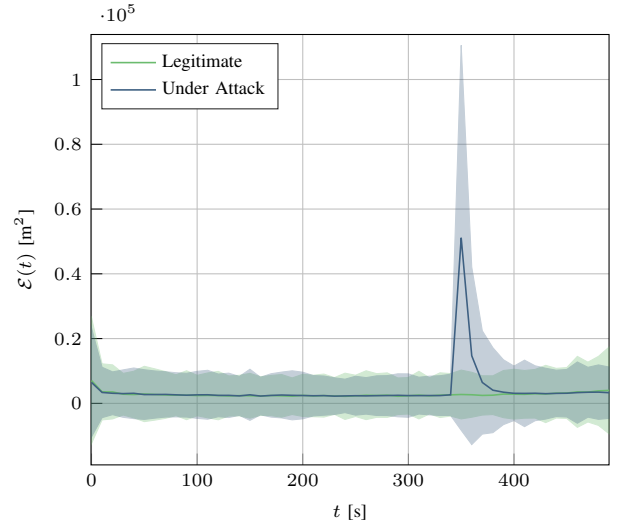


Fig. 13: Mean and 2σ confidence intervals of $\mathcal{E}(t)$, for RNN in the legitimate and under-attack (starting from $t = 350$ s) scenarios, for SNR = 20 dB.

D. Authentication Results

In this Section, we report the security performance of the proposed protocol, in terms of the squared error defined in (6).

We run 1000 simulations, half for legitimate and half for the under-attack scenario. Each simulation contains the trajectory sampled with period $T = 10$ s, using $N_{\text{rx}} = 50$ receivers (unless differently specified). Concerning the under-attack scenario, we considered that for $t < \ell T$ the transmission is legitimate, while for $t \geq \ell T$ Bob receives signals from Eve only, with $\ell = 35$.

More in detail, we consider a scenario where Eve partially localizes Alice, places herself at $D = 500$ m from Alice, and tries to replicate her motion pattern. Specifically, when Eve starts transmitting,

- her position is drawn at random at a distance of 500 m from Alice's last position;

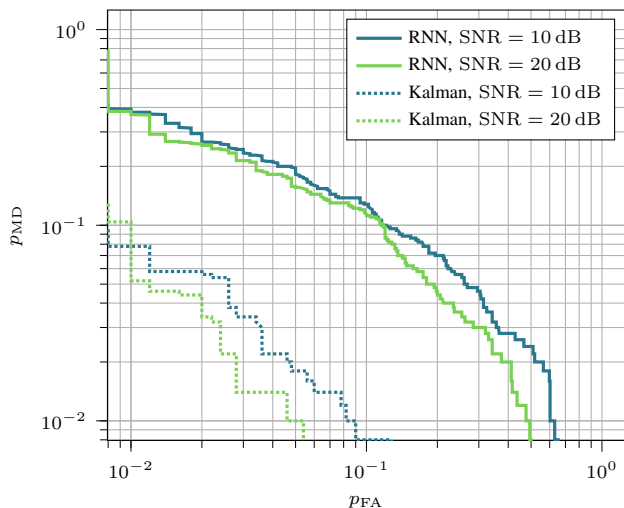


Fig. 14: Detection error tradeoff (DET) curves for the proposed Kalman and RNN based position predictors, for SNR = 10 and 20 dB.

- her initial speed is $v(0) = 1$ m/s;
- the angle of her initial motion direction with respect to the positive x -axis is uniformly sampled in the interval $[\phi - \frac{\pi}{4}, \phi + \frac{\pi}{4}]$, where ϕ is Alice's motion direction angle;
- her next positions are defined by the motion model in (29).

To show the distribution of $\mathcal{E}(t)$, for each time t Fig.s 12 and 13 show an interval having as endpoints $\mu - 2\sigma$ and $\mu + 2\sigma$, with μ being the average and σ being the standard deviation of the squared error distribution. Assuming the data to be Gaussian, the interval contains approximately 95% of the data. The two figures are obtained using the Kalman filter and the RNN, respectively, for position prediction; both figures are obtained with SNR = 20 dB.

As expected, in both Fig.s 12 and 13, the legitimate $\mathcal{E}(t)$ remains almost constant over time, while as the attack starts at $t = 350$ s we see a peak. Thus, both techniques can detect the attack and are suitable for authentication purposes. However, there are relevant differences between the two position predictor implementations. In particular, due to the previously-mentioned sensitivity to noise on input positions, differently from the Kalman filter the 2σ intervals in the legitimate and under-attack case are not separable when using the RNN.

To further investigate how such non-separability between the legitimate and under-attack $\mathcal{E}(t)$ affects the two predictors' ability to distinguish between Alice and Eve, Fig. 14 shows the DET curves, i.e., the MD probability p_{MD} (8) as a function of the FA probability p_{FA} (9) for SNR = 10 and 20 dB. The results are obtained using $N_a = 10$, meaning that the decision $\hat{\mathcal{H}}(t)$ is taken only after $t > 100$ s. We also tested other values of N_a , concluding that this parameter has a negligible impact on the performance. As expected, for both implementations better results are achieved at a higher SNR. Still, the Kalman filter outperforms the RNN and achieves p_{FA} and p_{MD} values of 0.024 while the latter cannot reach values lower than 0.1 for both probabilities. These results are consistent with the previously presented $\mathcal{E}(t)$ for the Kalman filter and the RNN,

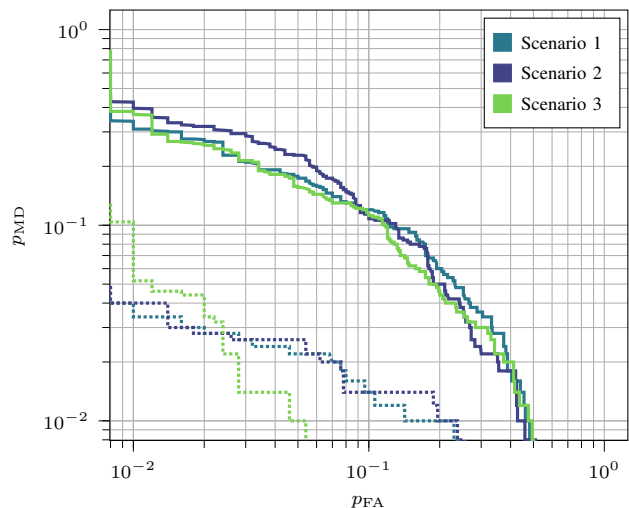


Fig. 15: DET curves for the proposed RNN and Kalman (dotted) based position predictors for SNR = 20 dB. In scenarios 1 and 2 environmental variability is considered for bathymetries 1 and 2, while scenario 3 is a reference with no environmental variability for bathymetry 1.

as the regularization imposed by the Kalman filter improves the detection of jumps on the position estimation. On the other hand, the RNN is trained to be robust to these inconsistencies, making room for Eve to lead a successful attack.

To address the variability of environmental conditions, we modify the Thorp absorption coefficient as a function of various parameters. More in detail, water's salinity, temperature, and pH take values respectively in [30ppt, 35ppt], [12°C, 24°C], and [6, 9]. By changing these parameters for each testing trajectory, we obtained the authentication performance shown in Fig. 15 for both available bathymetries. Note that the network has been trained on a single set of parameters, thus we are assessing its robustness against variations of the parameters with respect to the training phase. As expected, the environmental variability affects the LOC-NET accuracy and, consequently, the authentication performance. However, our model is robust even to high variations of the considered parameters.

UWAN can vary greatly in size and number of nodes, thus we tested the proposed authentication method scalability by varying the number of available receivers. Fig.s 16 and 17 show that our model is affected by the reduction of the available receivers, nonetheless achieving acceptable authentication performances even with as few as $N_{rx} = 20$.

As for the localization task, we tested the authentication performances removing the dependency on the LOC-NET estimates by generating transmitter positions as in (30) with $\sigma_{pos} = 25, 50, \text{ and } 100$ m. To do so, we generated 1000 source trajectories, half for the legitimate and half for the under-attack scenario, for each STD value. The generated trajectories are then fed to the Kalman filter and the trained RNN to extract $\mathcal{E}(t)$.

In Fig. 18, are plotted the DET curves representing the p_{MD} and the p_{FA} for the Kalman filter, the RNN and for different values of the added Gaussian noise STD. When $\sigma_{pos} = 100$ m

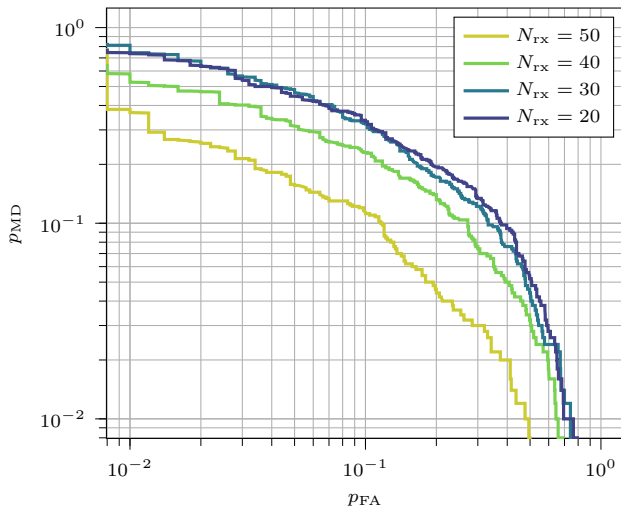


Fig. 16: DET curves for the RNN based position predictor with varying number of available receivers and SNR = 20 dB.

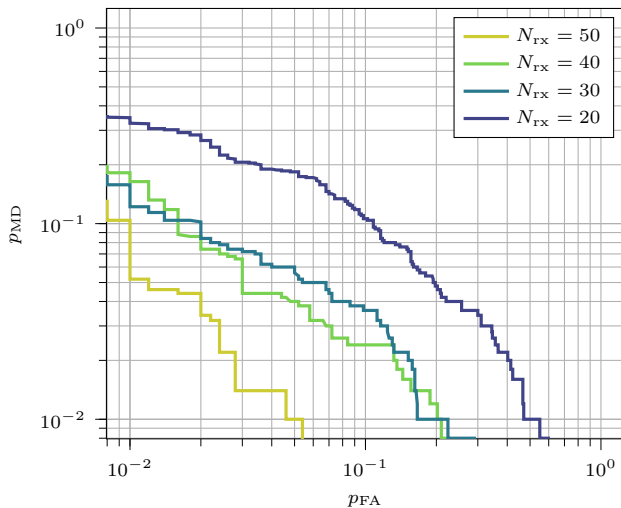


Fig. 17: DET curves for the Kalman-based position predictor with varying the number of available receivers and SNR = 20 dB.

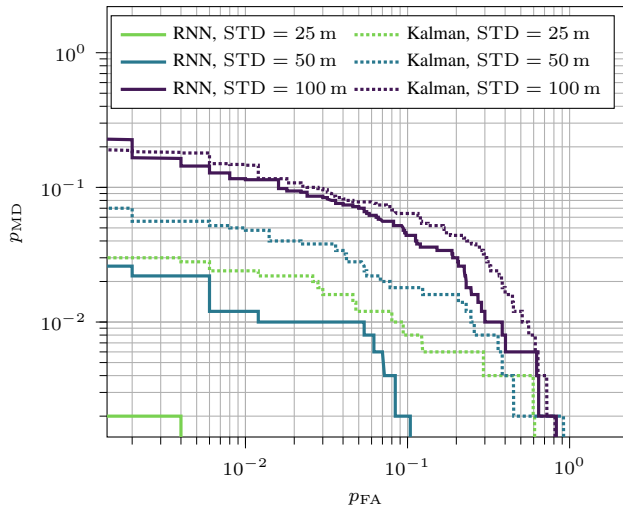


Fig. 18: DET simulated positions with additive Gaussian noise.

the performances of the two models are almost the same. However, decreasing the noise STD, the RNN outperforms the Kalman filter. This is because the noise samples added to the simulated positions, are uncorrelated between them while this is not the case for the LOC-NET errors. In fact, LOC-NET errors depend on the source location within the transmitter area therefore, the errors during one trajectory are correlated.

This error correlation favors the Kalman filter which can approximate the noisy trajectory with a constant speed motion model. On the other hand, having uncorrelated additive noise makes it more difficult to approximate the noisy trajectory with a constant speed motion model resulting in a less precise authentication metric $\mathcal{E}(t)$, which finally leads to higher p_{MD} and p_{FA} . The RNN instead, not having any prior assumption on the motion model, performs very well, especially with lower noise STD. In conclusion, when the sea is calm and the source moves at a constant speed (at least with a good approximation), the Kalman filter is the best solution. On the other hand, in rough seas or when the source undergoes sudden acceleration, the RNN should be preferred. In addition, while the Kalman filter typically outperforms the RNN, this is more robust at lower SNR, with fewer receivers, and under higher environmental variability. Thus, these conditions should also be considered together with the source type of motion when choosing the position predictor.

V. CONCLUSION

We have proposed a context-based authentication for UWANs, where an array of receivers aims at authenticating a moving transmitter relying on the physical properties of the underwater acoustic channel. The proposed approach is divided into two steps. First, we estimate the source coordinates by using the LOC-NET, a novel CNN developed for this task, which leverages the SCM obtained by combining the receivers' channel measurements. Next, we use a position predictor to track the evolution of the source position. As a predictor, we have considered both a Kalman filter and a RNN.

Finally, the security check relies on the comparison between the measured position with the predicted one, thus associating high position prediction errors with fake signals. The performance of the proposed scheme has been evaluated using a dataset collected from a Bellhop simulator. Results show that indeed the proposed scheme can distinguish between legitimate and fake signals while the transmitter is moving according to a realistic motion model.

Specifically, the Kalman filter achieves great results as long as the source motion can be approximated with a constant speed motion model. However, in scenarios where the source speed cannot be approximated as constant, the RNN would be a more appropriate predictor.

Future works include the implementation of a dynamic threshold for detection and a sea trial to evaluate the performance of the proposed scheme in a real-world context. This may include, for instance, marine life and geological features that cannot be modeled via simulation.

REFERENCES

- [1] C. Lal, R. Petrocchia, M. Conti, and J. Alves, "Secure underwater acoustic networks: Current and future research directions," in *Proc. 3rd IEEE Underwater Commun. and Networking Conf. (UComms)*, 2016, pp. 1–5.
- [2] G. Yang, L. Dai, G. Si, S. Wang, and S. Wang, "Challenges and security issues in underwater wireless sensor networks," in *Proc. of the Int. Conf. on Identification, Inf. and Knowl. in the Internet of Things (IIKI)*, vol. 147. Elsevier, 2019, pp. 210–216.
- [3] W. Aman, S. Al-Kuwari, M. Muzzammil, M. M. U. Rahman, and A. Kumar, "Security of underwater and air–water wireless communication: State-of-the-art, challenges and outlook," *Ad Hoc Networks*, vol. 142, pp. 103–114, Apr. 2023.
- [4] R. Diamant, P. Casari, and S. Tomasin, "Cooperative authentication in underwater acoustic sensor networks," *IEEE Trans. on Wireless Commun.*, vol. 18, no. 2, pp. 954–968, Dec. 2018.
- [5] M. Khalid, R. Zhao, and N. Ahmed, "Physical layer authentication in line-of-sight underwater acoustic sensor networks," in *Proc. of OCEANS*. Singapore: IEEE, 2020, pp. 1–5.
- [6] R. Zhao, M. Khalid, O. A. Dobre, and X. Wang, "Physical layer node authentication in underwater acoustic sensor networks using time-reversal," *IEEE Sens. J.*, vol. 22, no. 4, pp. 3796–3809, Jan. 2022.
- [7] R. Zhao, T. Shi, C. Liu, X. Shen, and O. A. Dobre, "Physical layer authentication without adversary training data in resource-constrained underwater acoustic networks," *IEEE Sens. J.*, vol. 23, no. 22, pp. 28 270–28 281, Nov. 2023.
- [8] L. Bragagnolo, F. Ardizzon, N. Laurenti, P. Casari, R. Diamant, and S. Tomasin, "Authentication of underwater acoustic transmissions via machine learning techniques," in *Proc. IEEE Int. Conf. on Microw., Antennas, Commun. and Electron. Syst. (COMCAS)*, 2021, pp. 255–260.
- [9] J. Du, G. Han, C. Lin, and M. Martínez-García, "LTrust: An adaptive trust model based on LSTM for underwater acoustic sensor networks," *IEEE Trans. on Wireless Commun.*, vol. 21, no. 9, pp. 7314–7328, Sept. 2022.
- [10] M. Zhang, R. Feng, H. Zhang, and Y. Su, "A recommendation management defense mechanism based on trust model in underwater acoustic sensor networks," *Future Gener. Comput. Syst.*, vol. 145, pp. 466–477, Aug. 2023.
- [11] P. Casari, F. Ardizzon, and S. Tomasin, "Physical layer authentication in underwater acoustic networks with mobile devices," in *Proc. of the 16th Int. Conf. on Underwater Networks & Systems (WUWNet)*, 2022.
- [12] F. Ardizzon, P. Casari, and S. Tomasin, "A RNN-based approach to physical layer authentication in underwater acoustic networks with mobile devices," *Comput. Netw.*, vol. 243, p. 110311, Apr. 2024.
- [13] W. Aman, S. Al-Kuwari, and M. Qaraqe, "A novel physical layer authentication mechanism for static and mobile 3D underwater acoustic communication networks," *Physical Communication*, vol. 66, p. 102430, Oct. 2024.
- [14] A. Sazontov and A. Malekhanov, "Matched field signal processing in underwater sound channels," *Acoustical Physics*, vol. 61, pp. 213–230, Mar. 2015.
- [15] M. B. Porter, "Bellhop Gaussian beam/finite element beam code," <http://oalib.hlsresearch.com/Rays/>, (Last access August 2024).
- [16] H. Niu, E. Reeves, and P. Gerstoft, "Source localization in an ocean waveguide using supervised machine learning," *The Jour. of the Acoustical Society of America*, vol. 142, no. 3, pp. 1176–1188, Sept. 2017.
- [17] Y. Wang and H. Peng, "Underwater acoustic source localization using generalized regression neural network," *The Jour. of the Acoustical Society of America*, vol. 143, no. 4, pp. 2321–2331, Apr. 2018.
- [18] Z. Huang, J. Xu, Z. Gong, H. Wang, and Y. Yan, "Source localization using deep neural networks in a shallow water environment," *The Jour. of the Acoustical Society of America*, vol. 143, no. 5, pp. 2922–2932, May 2018.
- [19] W. Liu, Y. Yang, M. Xu, L. Lü, Z. Liu, and Y. Shi, "Source localization in the deep ocean using a convolutional neural network," *The Jour. of the Acoustical Society of America*, vol. 147, no. 4, pp. 314–319, Apr. 2020.
- [20] Y. Liu, H. Niu, and Z. Li, "A multi-task learning convolutional neural network for source localization in deep ocean," *The Jour. of the Acoustical Society of America*, vol. 148, no. 2, pp. 873–883, Aug. 2020.
- [21] P.-F. Lv, B. He, and J. Guo, "Position correction model based on gated hybrid RNN for AUV navigation," *IEEE Trans. on Vehicular Technology*, vol. 70, no. 6, pp. 5648–5657, May 2021.
- [22] D. Qin, J. Tang, and Z. Yan, "Underwater acoustic source localization using LSTM neural network," in *Proc. of the 39th Chinese Control Conference (CCC)*. IEEE, 2020, pp. 7452–7457.
- [23] X. Zhu, H. Dong, P. S. Rossi, and M. Landrø, "Time-frequency fused underwater acoustic source localization based on contrastive predictive coding," *IEEE Sensors Journal*, vol. 22, no. 13, pp. 13 299–13 308, June 2022.
- [24] F. Chollet, "Xception: Deep learning with depthwise separable convolutions," in *Proc. of the Conf. on Comput. Vis. and Pattern Recognit. (CVPR)*, July 2017.
- [25] S. Ioffe and C. Szegedy, "Batch normalization: Accelerating deep network training by reducing internal covariate shift," in *Proc. Int. Conf. on machine learning*, 2015, pp. 448–456.
- [26] W. Hao, W. Yizhou, L. Yaqin, and S. Zhili, "The role of activation function in CNN," in *Proc. 2nd IEEE Int. Conf. on Inf. Technol. and Comput. Appl. (ITCA)*, 2020, pp. 429–432.
- [27] N. Srivastava, G. Hinton, A. Krizhevsky, I. Sutskever, and R. Salakhutdinov, "Dropout: a simple way to prevent neural networks from overfitting," *Jour. of Machine Learning Research*, vol. 15, no. 1, pp. 1929–1958, June 2014.
- [28] G. Welch and G. Bishop, "An introduction to the Kalman filter," *Technical report TR95-041*, 1995.
- [29] S. Kay, *Fundamentals of Statistical Signal Processing: Estimation Theory*. Englewood Cliffs, NJ: Prentice-Hall, 1993.
- [30] H. Sak, A. Senior, and F. Beaufays, "Long short-term memory based recurrent neural network architectures for large vocabulary speech recognition," *arXiv*, Feb. 2014.
- [31] P. B. Weerakody, K. W. Wong, G. Wang, and W. Ela, "A review of irregular time series data handling with gated recurrent neural networks," *Neurocomputing*, vol. 441, pp. 161–178, June 2021.
- [32] M. B. Porter and Y.-C. Liu, "Finite-element ray tracing," *Theoretical and computational acoustics*, vol. 2, pp. 947–956, Oct. 1994.



Gianmaria Ventura (Student Member, IEEE) received the B.Sc. degree in Information Engineering and the M.Sc. degree in Telecommunications Engineering from the University of Padova, Italy, in 2021 and 2023 respectively, where he is currently pursuing the Ph.D. degree in Information Engineering with the Department of Information Engineering, under the supervision of Prof. M. Rossi. His current research interests include authentication techniques for physical layer security and wireless joint communications and sensing.



Francesco Ardizzon (Member, IEEE) received the B.Sc. degree in 2016, the M.Sc. degree in 2019, and the Ph.D. degree in Information Engineering in 2023 from the University of Padova, Italy. In 2022 he was a visiting scientist at the ESA European Space Research and Technology Centre. He is currently an Assistant Professor at the University of Padova. His current research interests include authentication for global navigation satellite systems, physical layer security, and underwater acoustic communications.



Stefano Tomasin (Senior Member, IEEE) received a Ph.D. degree from the University of Padova, Italy, in 2003. He joined the University of Padova where he is now Full Professor (since 2022). He was visiting faculty at Qualcomm, San Diego (CA) in 2004, the Polytechnic University in Brooklyn (NY) in 2007, and the Mathematical and Algorithmic Sciences Laboratory of Huawei in Paris (France) in 2015. His current research interests include physical layer security, security of global navigation satellitesystems, signal processing for wireless communications, synchronization, and scheduling of communication resources. He has been a senior member of IEEE since 2011 (member since 1999) and a member of EURASIP since 2011. He is a Deputy Editor-in-Chief of the IEEE Transactions on Information Forensics and Security since January 2023.